Chimeric Small Subunits Influence Catalysis without Causing Global Conformational Changes in the Crystal Structure of Ribulose-1,5-bisphosphate Carboxylase/Oxygenase[†,‡]

Saeid Karkehabadi,[§,||] Srinivasa R. Peddi,[§,⊥,#] M. Anwaruzzaman,[⊥,△] Thomas C. Taylor,[||] Andreas Cederlund,[||] Todor Genkov,[⊥] Inger Andersson,[||] and Robert J. Spreitzer*[,⊥]

Department of Biochemistry, University of Nebraska, Lincoln, Nebraska 68588, and Department of Molecular Biology, Swedish University of Agricultural Sciences, 751 24 Uppsala, Sweden

Received March 23, 2005; Revised Manuscript Received May 17, 2005

ABSTRACT: Comparison of subunit sequences and X-ray crystal structures of ribulose-1,5-bisphosphate carboxylase/oxygenase indicates that the loop between β-strands A and B of the small subunit is one of the most variable regions of the holoenzyme. In prokaryotes and nongreen algae, the loop contains 10 residues. In land plants and green algae, the loop is comprised of ∼22 and 28 residues, respectively. Previous studies indicated that the longer βA−βB loop was required for the assembly of cyanobacterial small subunits with plant large subunits in isolated chloroplasts. In the present study, chimeric small subunits were constructed by replacing the loop of the green alga *Chlamydomonas reinhardtii* with the sequences of *Synechococcus* or spinach. When these engineered genes were transformed into a *Chlamydomonas* mutant that lacks small-subunit genes, photosynthesis-competent colonies were recovered, indicating that loop size is not essential for holoenzyme assembly. Whereas the *Synechococcus* loop causes decreases in carboxylation V_{max}, $K_m(O_2)$, and CO_2/O_2 specificity, the spinach loop causes complementary decreases in carboxylation V_{max}, $K_m(O_2)$, and $K_m(CO_2)$ without a change in specificity. X-ray crystal structures of the engineered proteins reveal remarkable similarity between the introduced βA−βB loops and the respective loops in the *Synechococcus* and spinach enzymes. The side chains of several large-subunit residues are altered in regions previously shown by directed mutagenesis to influence CO_2/O_2 specificity. Differences in the catalytic properties of divergent Rubisco enzymes may arise from differences in the small-subunit βA−βB loop. This loop may be a worthwhile target for genetic engineering aimed at improving photosynthetic CO_2 fixation.

Because ribulose-1,5-bisphosphate carboxylase/oxygenase (Rubisco,[1] EC 4.1.1.39) catalyzes the rate-limiting step of photosynthetic CO_2 fixation, there has been much interest in engineering its rate of carboxylation or CO_2/O_2 specificity as a means for increasing agricultural productivity (reviewed in refs *1*−*5*). Whereas carboxylation of RuBP generates two molecules of 3-phosphoglycerate, competitive oxygenation of RuBP, which is a nonessential process, generates one molecule of 3-phosphoglycerate and one molecule of phosphoglycolate. Phosphoglycolate enters the photorespiratory pathway that leads to the loss of CO_2. Thus, an engineered increase in the catalytic efficiency (V_{max}/K_m) of carboxylation or a decrease in that of oxygenation would result in an increase in net CO_2 fixation. The CO_2/O_2 specificity factor kinetic constant, termed Ω, is defined as the ratio of these catalytic efficiencies, V_cK_o/V_oK_c, where V is the V_{max} of either carboxylation or oxygenation and K is the Michaelis constant for CO_2 or O_2 (*6*). The Ω values of Rubisco enzymes from diverse species are substantially different (*7*−*10*), but it is difficult to tell whether any of these enzymes is "better" (*1*, *11*) because there is an inverse correlation between V_c and Ω (*7*), and intracellular CO_2 and O_2 concentrations vary considerably among species (*12*, *13*).

X-ray crystal structures of Rubisco enzymes are all quite similar when Cα traces are compared (reviewed in ref *2*). Two ∼55 kDa large subunits assemble into functional dimers with two active sites (Figure 1A). Loops of the carboxyl-terminal α/β-barrel domain of one subunit and the amino-terminal domain of the other contribute conserved residues that interact with the carboxylation transition state analogue CABP. Four ∼15 kDa small subunits cap the top and bottom

[†] This work was supported by the U.S. Department of Energy (Award DE-FG02-00ER15044), Nebraska Agricultural Research Division (Journal Series Paper 14948), Swedish Research Council for Environment, Agricultural Sciences, and Spatial Planning (FORMAS), and European Union (QLK3-CT-2002-01945).

[‡] Coordinates and structure factors have been deposited in the Protein Data Bank with accession codes 1UZH for the ABAN mutant and 1UZD for the ABSO mutant enzymes.

* To whom correspondence should be addressed. Tel: 402-472-5446. Fax: 402-472-7842. E-mail: rspreitzer1@unl.edu.

[§] These authors contributed equally to this research.

[||] Swedish University of Agricultural Sciences.

[⊥] University of Nebraska.

[#] Current address: Stanley S. Scott Cancer Center, Louisiana State University Health Sciences Center, New Orleans, LA 70112.

[△] Current address: Department of Plant and Microbial Biology, University of California, Berkeley, CA 94720-3102.

[1] Abbreviations: Rubisco, ribulose-1,5-bisphosphate carboxylase/oxygenase; RuBP, D-ribulose 1,5-bisphosphate; Ω, CO_2/O_2 specificity factor; CABP, 2-carboxy-D-arabinitol 1,5-bisphosphate; SDS, sodium dodecyl sulfate.

10.1021/bi050537v CCC: $30.25
Published on Web 06/25/2005

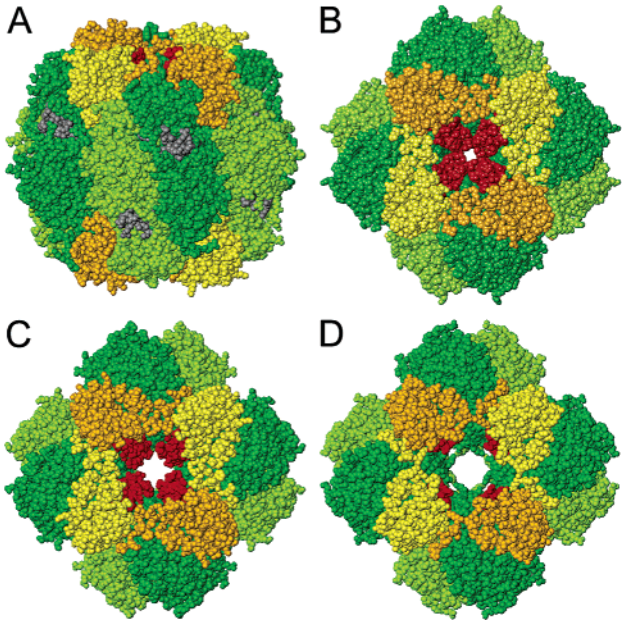

FIGURE 1: Comparison of Rubisco X-ray crystal structures: (A) green alga *C. reinhardtii* (1GK8) side view tilted 30° forward around the *X* axis (*14*), (B) *Chlamydomonas* top view, (C) land plant spinach (*S. oleracea*) (8RUC) top view (*15*), and (D) cyanobacterium *Synechococcus* (*A. nidulans*) (1RBL) top view (*16*). Large subunits that form functional dimers are colored light and dark green. Small subunits are colored yellow and orange. Loops between large-subunit β-strand 6 and α-helix 6 are colored gray to denote the active sites. Loops between small-subunit β-strands A and B are colored red.

of four pairs of the large subunits to form the hexadecameric holoenzyme. The most notable difference among various Rubisco enzymes occurs in the loop between β-strands A and B of the small subunit (Figure 1) (*14*−*17*). The βA−βB loops of four small subunits reside at each end of the solvent channel that traverses the holoenzyme. Cyanobacteria have only 10 residues in the loop, but land plants have as many as 22 and green algae have 28 (reviewed in ref *5*). Nongreen algae and some prokaryotes, which also have only 10 residues in their βA−βB loops, have carboxyl-terminal extensions that form β-hairpin structures in the spaces that are normally occupied by the longer βA−βB loops of green algal and land plant enzymes (*18*, *19*). Considering that some prokaryotic Rubisco enzymes lack small subunits (reviewed in refs *2* and *5*), and these dimeric large-subunit holoenzymes have the lowest Ω values (*7*), one wonders whether the variation in the small-subunit βA−βB loop plays a role in the differences in V_c and Ω observed among different Rubisco enzymes.

When the 10-residue βA−βB loop of the cyanobacterium *Synechococcus* was replaced with the 22-residue loop of pea (*Pisum sativum*), the *Synechococcus* small subunit was now able to assemble with pea large subunits in isolated chloroplasts (*20*). Subsequent directed mutagenesis and chloroplast import showed that an R53E substitution in the pea βA−βB loop was particularly detrimental to holoenzyme assembly (*21*, *22*). These studies indicated that the longer βA−βB loop may play a role in assembly, but it was difficult to assess whether the extra residues in the land plant loop might affect catalysis. Land plant Rubisco cannot assemble in *Escherichia coli* (*23*), and because land plants have a family of *rbcS* small-subunit genes in the nucleus (reviewed in ref *5*), it has not been possible to create a suitable host for transformation of engineered small subunits in vivo (*24*−*26*).

More recently, N54S and A57V small-subunit substitutions in the βA−βB loop were selected in the green alga *Chlamydomonas* as suppressor mutations that restore the decreases in V_c, Ω, and thermal stability that result from an L290F substitution in the large subunit (*27*, *28*). To further investigate the functional significance of the loop, a *Chlamydomonas* mutant that lacks the *rbcS* gene family (*29*) and requires acetate for growth was used as a host for transformation (*30*). Five βA−βB-loop residues that are conserved among green algae and land plants but missing or different in the shorter βA−βB loops of prokaryotes and nongreen algae were each substituted with Ala. None of these substitutions (R59A, Y67A, Y68A, D69A, and R71A) blocked photosynthetic growth, and only the R71A substitution caused a substantial decrease in holoenzyme thermal stability in vivo and in vitro (*30*). When an R59E enzyme was created, to mimic the R53E enzyme of land plants (*21*, *22*), Rubisco also assembled in *Chlamydomonas*, albeit at a lower level and with an associated decrease in thermal stability (*30*). More importantly, the Y68A and D69A enzymes had lower K_c values, which were offset by decreases in V_c, and the R71A enzyme had an 8% decrease in Ω due to a decrease in V_c and increase in K_c (*30*). Thus, none of these substitutions eliminated holoenzyme assembly in vivo, but two affected catalytic efficiency (Y68A and D69A) and one caused a decrease in Ω (R71A).

When the X-ray crystal structure of *Chlamydomonas* Rubisco was solved (*14*), it became clear that sequence alignment of the βA−βB loop was not the same as structural alignment. For example, whereas Arg59 of *Chlamydomonas* was thought to be homologous with Arg53 of land plants (*30*), the X-ray crystal structure revealed that the backbone atoms of Asn54 in *Chlamydomonas* align with those of Arg53 in spinach. However, the guanidino group of Arg59 from a neighboring small subunit of *Chlamydomonas* is in perfect structural alignment with the guanidino group of Arg53 in the same small subunit of spinach (*14*). Furthermore, the *Chlamydomonas* N54S and A57V suppressor substitutions (*28*) reside in a region of the βA−βB loop unique to plant and green algal enzymes. Therefore, to better understand the role of structural divergence in the βA−βB loop, the *Chlamydomonas* loop was replaced with the shorter loops of spinach and *Synechococcus* in the present study. Both mutant strains can grow photoautotrophically, indicating that species-specific differences in the loops are not essential for holoenzyme assembly. However, both mutant enzymes have altered catalytic properties, and the introduction of the *Synechococcus* loop causes an 11% decrease in Ω. Despite these changes in catalysis, X-ray crystal structures reveal remarkable conservation of cyanobacterial and land plant βA−βB-loop structures in the algal large-subunit environment.

MATERIALS AND METHODS

Strains and Culture Conditions. Chlamydomonas reinhardtii 2137 *mt*$^+$ is the wild-type strain (*31*). Mutant *rbcS*Δ-T-60 was used as the host for nuclear transformation. It lacks photosynthesis and requires acetate for growth due to deletion of the 13-kb locus that contains the small-subunit *rbcS1* and

rbcS2 genes (*29*). All *Chlamydomonas* strains are maintained at 25 °C in darkness with 10 mM acetate medium containing 1.5% Bacto agar (*31*). For routine biochemical analysis, cells were grown on a rotary shaker at 220 rpm with 250−500 mL of liquid acetate medium in darkness.

Construction of Chimeric Genes. A 17 base pair *Sma*I/*Hin*cII DNA fragment was deleted from plasmid pUC19 (*32*) to generate pUC19Δ, which lacks *Sma*I, *Bam*HI, *Xba*I, and *Hin*cII restriction enzyme sites. The 5 kilobase pair *Eco*RI fragment of pSS1 (*29*), which contains the wild-type *Chlamydomonas rbcS1* gene at the *Eco*RI site of pUC19, was subcloned into *Eco*RI-digested pUC19Δ to create plasmid pΔSS1. Sequences encoding small-subunit βA−βB-loop regions were amplified from *Chlamydomonas rbcS1* with forward primers for spinach (5′-GGCTGGATCCCCT-GCCTGGAGTTCGCT ACC GAC CAC GGT TTC GTG TAC CGC GAG CAC CAC AAC AGC CCC GGT TAC TAC GAC GGT CGC TAC TGG-3′) or *Synechococcus* (5′-GGCTGGATCCCCTGCCTGGAGTTCGCT GAG CAC AGC AAC CCC GAG GAA TTC TAC TGG-3′) and a reverse primer encompassing the unique *Stu*I site of the *Chlamydomonas rbcS1* gene. Unique *Msp*I (CCCCGG) and *Eco*RI (GAATTC) sites were also engineered in the spinach and *Synechococcus* sequences, respectively, and codons were introduced that are common to the nuclear gene products of *Chlamydomonas*. Because both of the forward primers have identical 5′ sequences encompassing a unique *Bam*HI (GGATCC) site in the region encoding *Chlamydomonas* β-strand A, the amplified products were digested with *Bam*HI and *Stu*I, and the resulting *Bam*HI/*Stu*I fragments were used to replace the *Bam*HI/*Stu*I fragment of pΔSS1. These final constructs eliminate intron 3 of *rbcS1* and encode proteins in which the βA−βB loops of spinach or *Synechococcus* are inserted precisely between β-strands A and B of the *Chlamydomonas* small subunit. The chimeric *rbcS1* genes were confirmed by *Msp*I and *Eco*RI restriction enzyme digestion. The plasmids encoding the βA−βB loops of spinach (*Spinacea oleracea*) and *Synechococcus* (*Anacystis nidulans*) were named pSS1-ABSO and pSS1-ABAN, respectively.

Transformation and Mutant Recovery. Dark-grown *rbcS*Δ-T60-3 cells were concentrated by centrifugation to 4×10^8 cells/mL. Electroporation transformation (*33*) was performed with a Bio-Rad Gene Pulser Xcell electroporation system using a 4 mm gap cuvette (Equibio, Kent, U.K.) containing 2.5 μg of plasmid DNA and 1×10^8 cells in 0.25 mL of 50 mM sucrose in acetate medium. The cells, which lack the cell wall (*29*), were electroporated at 750 V with 25 μF capacitance. They were then transferred to 50 mL of acetate medium in a 250 mL Delong flask and cultured in darkness for 16 h. To select transformants, the cells were concentrated by centrifugation and plated on minimal medium in the light (80 μmol of photons m^{-2} s^{-1}) at a density of 2×10^6 cells per 100 mm Petri plate. Total DNA was extracted from the photosynthesis-competent transformants (*34*), and the *rbcS* gene was amplified by the polymerase chain reaction (*29*). The amplified DNA was completely sequenced at the DNA sequencing facility of the University of Nebraska (Lincoln, NE) to verify that only the expected changes were present. The mutant strains containing *Synechococcus* (*A. nidulans*) and spinach (*S. oleracea*) small-subunit βA−βB-loop insertions were named ABAN and ABSO, respectively.

Biochemical Analysis. Approximately 1×10^9 cells were harvested by centrifugation, resuspended in 1.5 mL of 50 mM *N*,*N*-bis(2-hydroxyethyl)glycine (pH 8.0), 10 mM $NaHCO_3$, 10 mM $MgCl_2$, and 1 mM dithiothreitol, and sonicated at 0 °C for 3 min. Cell debris was removed by centrifugation at 37000*g* for 15 min, and the amount of proteins in the resulting cell extract was determined by the method of Bradford (*35*). The cell extract was then subjected to sucrose gradient centrifugation to purify Rubisco holoenzyme (*36*) or fractionated by SDS−polyacrylamide gel electrophoresis for western analysis (*37*). Proteins were transferred from the gel to the nitrocellulose membrane, probed with rabbit anti-*Chlamydomonas* Rubisco immunoglobulin G, and detected by chemiluminescence (*38*). Antibodies were affinity purified (*39*) from serum kindly provided by Dr. Arminio Boschetti (University of Bern, Bern, Switzerland).

Thermal stability was assayed by incubating 5 μg of purified and activated enzyme in 0.5 mL of 50 mM *N*,*N*-bis(2-hydroxyethyl)glycine (pH 8.0), 10 mM $NaHCO_3$, 10 mM $MgCl_2$, and 1 mM dithiothreitol at various temperatures for 10 min (*40*). The samples were then cooled on ice for 5 min, and carboxylase activity was assayed at 25 °C by adding 50 μL of the incubated enzymes to 450 μL of assay buffer containing 50 mM *N*,*N*-bis(2-hydroxyethyl)glycine (pH 8.0), 0.4 mM RuBP, 10 mM $NaH^{14}CO_3$ (2 Ci/mol), and 10 mM $MgCl_2$. After 1 min, the reactions were terminated by adding 0.5 mL of 3 M formic acid in methanol. Samples were dried at 80 °C for 10 h, and incorporation of ^{14}C was measured by liquid scintillation counting.

The carboxylation and oxygenation kinetic constants of purified and activated enzyme were assayed by measuring the incorporation of acid-stable ^{14}C from $NaH^{14}CO_3$ (*27*). Ω was determined with 20 μg of Rubisco per reaction by assaying carboxylase and oxygenase activities simultaneously with 130 μM [1-^{3}H]RuBP (7.2 Ci/mol) and 2 mM $NaH^{14}CO_3$ (0.5 Ci/mol) in 30 min reactions at 25 °C (*41*, *42*). Phosphoglycolate phosphatase and [1-^{3}H]RuBP were synthesized/purified according to standard methods (*41*, *43*).

Crystallization and Structure Determination. For large-scale production of Rubisco, cells were grown with 3−5 L of acetate medium in darkness, harvested by centrifugation at 2500*g* for 5 min, and lysed by sonication. After differential ammonium sulfate precipitation between 30% and 50% saturation, the redissolved cellular protein was loaded onto a Superdex-200 16/60 size exclusion column. The fractions corresponding to Rubisco were collected and loaded onto a Mono Q anion-exchange column. Rubisco was eluted from the column with a 0.1−0.5 M NaCl gradient. Crystals of mutant Rubisco were grown using hanging-drop vapor diffusion at 20 °C. The drops were prepared by mixing a solution containing 10 mg/mL Rubisco and 1 mM CABP with an equal volume of a well solution containing 50 mM HEPES (pH 7.5), 50−200 mM NaCl, 7−12% poly(ethylene glycol) 4000, 10 mM $NaHCO_3$, and 5 mM $MgCl_2$. Crystals grew within 1 week. Prior to data collection, crystals were transferred to a solution containing the well solution with 30% ethylene glycol as a cryoprotectant and frozen in liquid N_2. Data were collected from single crystals at 100 K on beam line ID29 at the European Synchrotron Radiation Facility, Grenoble, France. The data were processed using DENZO and SCALEPACK (*44*) to a resolution of

```
                 40   45   50   55   60   65   70   75
Chlamydomonas IPCLEFAEADKAYVSNESA-IRFGSVSCLYYDNRYWTMW
                 40   45   50   55        60   65   70
Spinach       VPCLEFET-DHGFVYREHHN------SPGYYDGRYWTMW
                 40   45   50                   55
Synechococcus HPLIEFNE--HSNPE----------------EFYWTMW
                 40   45   50   55        60   65   70
ABSO Chimera  IPCLEFAT-DHGFVYREHHN------SPGYYDGRYWTMW
                 40   45   50                   55
ABAN Chimera  IPCLEFAE--HSNPE----------------EFYWTMW
```

FIGURE 2: Sequences of Rubisco small-subunit βA−βB-loop regions of *Chlamydomonas*, spinach, *Synechococcus*, and the *Chlamydomonas* chimeric mutants ABSO and ABAN containing the βA−βB loops of spinach and *Synechococcus*, respectively. Hyphens are inserted to align the sequences according to the X-ray crystal structures (*14*−*16*). β-Stands A and B are shaded in gray.

2.2 Å for the ABAN and 2.4 Å for the ABSO mutant enzymes.

The mutant crystal structures were solved by molecular replacement using the program AMORE (*45*, *46*). The search model consisted of one set of large and small subunits of wild-type *Chlamydomonas* Rubisco (PDB code 1GK8) (*14*) in which the βA−βB loop of the small subunit had been removed. In each case, eight solutions corresponding to eight different orientations of the search unit within one hexadecamer in the asymmetric unit were found. Refinement was performed using REFMAC version 5 (*47*). For cross-validation, 5% of the data was excluded from the refinement for R_{free} calculations. Initial electron density maps calculated after one round of rigid body refinement showed clear density for the chimeric βA−βB loops. After building the corresponding loops into density, the mutant structures were further refined using a maximum likelihood target function with noncrystallographic symmetry restraints for the eight copies of large and small subunits in the asymmetric unit. Solvent molecules were added using ARP/wARP (*48*). Throughout the refinement, $2mF_o - DF_c$ and $mF_o - DF_c$ sigmaA-weighted maps (*49*) were inspected and the models manually adjusted using O (*50*). The structures of the ABAN and ABSO enzymes were refined to final R_{cryst}/R_{free} values of 0.165/0.195 and 0.195/0.225, respectively. Coordinates and structure factors have been deposited at the Protein Data Bank with accession codes 1UZH and 1UZD.

Calculation of Occluded Surface Area. The surface areas buried between the βA−βB loops and neighboring subunits were calculated using the occluded surface area algorithm as described by Pattabiraman et al. (*51*). Regions of the small-subunit loops were chosen, based on divergence of the small-subunit Cα traces, and compared beginning at residue 45 and ending at Tyr72 in *Chlamydomonas*, Tyr66 in spinach and mutant ABSO, and Tyr54 in *Synechococcus* and mutant ABAN. The occluded surface areas were calculated for each atom, and the total surface area occluded by neighboring subunits was summed over the entire sequence.

RESULTS

Recovery and Phenotypes of Mutants. To assess the significance of the variation in size of the small-subunit βA−βB loop, the 28-residue loop sequence of *Chlamydomonas*, which is representative of green algae, was replaced with the shorter loop sequences of spinach and *Synechococcus*, which are representative of land plants (22 residues) and prokaryotes (10 residues) (Figure 2). When the engineered pABSO (spinach) and pABAN (*Synechococcus*) chimeric *rbcS* plasmids were transformed into the *Chlamydomonas* *rbcS*Δ deletion mutant, photosynthesis-competent colonies arose on minimal medium in the light at frequencies of 8.4×10^{-5} and 8.0×10^{-5} cells, respectively. Because these frequencies are similar to that obtained with the wild-type *rbcS1* gene (9.3×10^{-5} cells), no significant deleterious effects of the shorter βA−βB loops were apparent. Furthermore, because the *rbcS1* genes in the pABSO and pABAN plasmids lack intron 3, it is apparent that this intron is not essential for *rbcS* mRNA expression. However, when the growth phenotypes of a number of pABSO and pABAN transformants were assessed in "spot tests" (*31*), all of the pABAN transformants failed to grow on minimal medium in the light at 35 °C. No other phenotypic difference relative to wild-type *rbcS1* transformants was observed on minimal medium at 25 °C or acetate medium in darkness at 25 or 35 °C. Despite the fact that the ABAN mutant strain has a temperature-conditional phenotype, the size of the βA−βB loop is clearly not essential for Rubisco assembly or function.

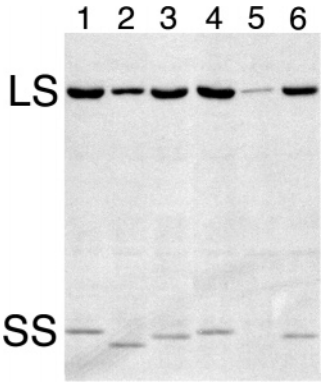

FIGURE 3: Western blot analysis of total soluble proteins from wild type (lanes 1 and 4), chimeric mutant ABAN (lanes 2 and 5), and chimeric mutant ABSO (lanes 3 and 6). Extracts (30 μg per lane) of cells grown at 25 (lanes 1−3) or 35 °C (lanes 4−6) with acetate medium in darkness were fractionated by SDS−polyacrylamide (7.5−15%) gradient gel electrophoresis (*37*). Proteins were blotted to nitrocellulose, probed with anti-*Chlamydomonas* Rubisco immunoglobulin G (0.5 μg/mL), and detected by enhanced chemiluminescence (*38*). The Rubisco large subunit (LS) and small subunit (SS) are indicated.

Thermal Stability of the Chimeric Rubisco Enzymes. When extracts of 25 °C grown cells were subjected to SDS−polyacrylamide gel electrophoresis and western analysis (Figure 3), mutant ABAN had only somewhat less Rubisco subunits than mutant ABSO or an *rbcS1* wild-type transformant, and the decreased molecular masses of the ABAN and ABSO small subunits agreed with the engineered decreases in the sizes of the βA−βB loops (Figure 2). However, in extracts of 35 °C grown cells, mutant ABAN had only a trace of Rubisco subunits (Figure 3), which would account for its inability to grow photosynthetically at 35 °C. Because unassembled Rubisco small subunits are rapidly degraded in *Chlamydomonas* (*52*), their abundance in cell extracts reflects the amount of holoenzyme in vivo. To further assess the stability of the chimeric mutant enzymes, Rubisco was purified from 25 °C grown cells and analyzed for its ability to retain RuBP carboxylase activity after incubation at various temperatures. As shown in Figure 4, ABAN Rubisco retained less activity than the wild-type enzyme, but ABSO Rubisco retained more activity than the wild-type enzyme. For example, in three separate experiments, ABAN Rubisco was completely inactivated after 10 min at 60 °C, but wild-

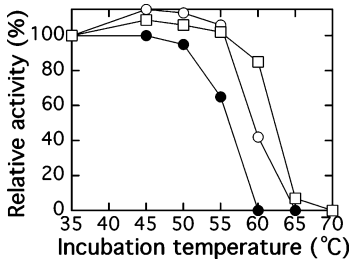

FIGURE 4: Thermal inactivation of Rubisco purified from wild type and chimeric small-subunit mutants. Rubisco was incubated at each temperature for 10 min. The samples were then cooled on ice, and RuBP carboxylase activity was assayed at 25 °C (*40*). Activities were normalized against activity measured after the 35 °C incubation. Key: wild-type transformant containing only the *RbcS1* gene (○), chimeric mutant ABAN (●), and chimeric mutant ABSO (□).

Table 1: Kinetic Properties of Rubisco Purified from Wild Type and Chimeric Mutants

kinetic constant	wild type	ABSO	ABAN
$\Omega = V_cK_o/V_oK_c$[a]	63 ± 2	62 ± 3	56 ± 1
V_c (μmol h^{-1} mg^{-1})[a]	111 ± 6	55 ± 4	60 ± 6
K_c (μM CO_2)[a]	35 ± 2	26 ± 3	36 ± 1
K_o (μM O_2)[a]	501 ± 18	431 ± 10	350 ± 2
V_c/K_c[b]	3.2	2.1	1.7
K_o/K_c[b]	14	17	10
V_c/V_o[b]	5.0	4.0	6.0

[a] Values are means ± standard deviation ($n - 1$) of three separate enzyme preparations. [b] Calculated values.

type and ABSO Rubisco retained 44 ± 2% and 85 ± 2% (±$n - 1$ standard deviation) of their initial activities, respectively, after incubation at the same temperature. Thus, although the nature of the βA−βB-loop sequence is not essential for holoenzyme assembly, it can influence holoenzyme stability in vivo and in vitro.

Kinetics of the Chimeric Enzymes. To assess the influence of the spinach (ABSO) and *Synechococcus* (ABAN) βA−βB loops on Rubisco function, the kinetic properties of the purified and activated chimeric enzymes were determined in detail (Table 1). Whereas the Ω value of the ABSO mutant enzyme is not significantly different from that of wild-type *Chlamydomonas* Rubisco, Ω of the ABAN enzyme is decreased by 11%. This decrease results primarily from a 46% decrease in V_c and 30% decrease in K_o, with no change in K_c. Although native *Synechococcus* Rubisco has a lower Ω than that of *Chlamydomonas* Rubisco (*7*), the substantial decrease in V_c indicates that the ABAN enzyme would have a lower net carboxylation rate than that of either wild-type enzyme (*6*). The ABSO enzyme also has decreases in V_c and K_o (50% and 14%, respectively), but these are offset by a 26% decrease in K_c (and an increase in K_o/K_c) (Table 1). A lower V_c and higher K_o/K_c are characteristic of spinach Rubisco, but the spinach enzyme has an Ω value greater than that of *Chlamydomonas* Rubisco (*7*). Because the ABSO enzyme has the same Ω value as wild-type *Chlamydomonas* Rubisco, the substantial decrease in V_c indicates that its net carboxylation would be lower than that of the wild-type *Chlamydomonas* or spinach enzymes. Despite some changes in kinetic properties that mimic those of the *Synechococcus* and spinach enzymes, it is difficult to tell from kinetics alone whether the foreign βA−βB loops impart catalytic properties of the *Synechococcus* and spinach enzymes or whether they cause deleterious effects due to global disruption of the holoenzyme structure.

Table 2: Statistics for Data Collection and Refinement

	ABSO	ABAN
resolution limit[a] (Å)	2.4	2.2
space group	$P2_12_12$	$P2_12_12$
cell dimensions *a*, *b*, *c* (Å)	220.0, 224.1, 111.8	220.8, 224.0, 112.0
no. of reflections		
measured	6104932	5695441
unique	215895	277345
completeness (%)	95.4 (96.1)[d]	90.2 (81.6)
I/σ	7.6 (1.4)	8.7 (2.0)
R_{merge}[b]	0.185 (0.780)	0.148 (0.444)
Wilson *B*-factor B_W[a] (Å^2)	31.8	21.2
R_{cryst}[c]	0.190 (0.25)	0.160 (0.21)
R_{free}[c]	0.230 (0.28)	0.190 (0.25)
estd coordinate error[a] (Å)	0.119	0.150
rmsd from ideal geometry		
bond lengths (Å)	0.014	0.014
bond angles (deg)	1.39	1.25

[a] For the wild-type *C. reinhardtii* Rubisco structure (PDB code 1GK8), the resolution limit is 1.4 Å, the Wilson *B*-factor is 11.8 Å^2, and the estimated coordinate error (based on maximum likelihood calculations) is 0.034 Å. [b] $R_{merge} = \sum_h\sum_i|I_i(h) - \langle I_i(h)\rangle|/\sum_h\sum_i I_i(h)$, where I is the observed intensity and $\langle I\rangle$ is the mean intensity of reflection h. [c] $R = \sum_{hkl}||F_o| - |F_c||/\sum_{hkl}|F_o|$, where F_o and F_c are the observed and calculated structure factor amplitudes, respectively. [d] Values in parentheses are for the highest resolution shell.

X-ray Crystal Structures of the Chimeric Enzymes. To determine whether the altered kinetic properties of the ABAN and ABSO mutant enzymes arose from either general misfolding of the small subunit or alterations in specific interactions with the large subunit, the purified proteins were crystallized, and their structures were determined. The crystallographic data collection and refinement statistics for the mutant enzyme crystal structures are summarized in Table 2. The quality of the structures is evidenced by the low R_{cryst} and R_{free} values and only minor deviations from ideal geometry. The final electron density maps for the ABSO enzyme show density for residues 11−475 (from a total of 475 residues) of the large subunit and residues 1−121 and 127−134 (from a total of 134 residues) for the small subunit. For ABAN, density is visible for residues 11−475 of the large subunit and residues 1−122 (from a total of 122 residues) for the small subunit. Clear density was observed for the chimeric loops in each case. As shown in Figure 5, the βA−βB loops of the ABAN and ABSO small subunits are remarkably similar to the native loops in the crystal structures of Rubisco from *Synechococcus* and spinach, respectively (*15*, *34*). No alteration is observed in the Cα backbone trace of the ABSO or ABAN large subunit when compared with the large subunit of wild-type *Chlamydomonas*. A superposition of the wild-type large subunit with the large subunits of ABSO and ABAN using the algorithms encoded in O (*50*) gave root-mean-square deviations of 0.211 and 0.157 Å for all Cα atoms, respectively.

Comparative Analysis of βA−βB Loop Structures. The βA−βB loop appears to be somewhat autonomous in assembly relative to holoenzyme structure. For example, with respect to the βA−βB loop of the ABSO enzyme, the guanidino group of Arg53 is positioned within the core of the loop as in spinach Rubisco rather than being contributed by a neighboring small subunit as in *Chlamydomonas* Rubisco (*14*). The only notable differences in arrangement of ABSO Cα backbone atoms relative to the spinach βA−βB loop are observed at residues Thr46, Asp47, and His48.

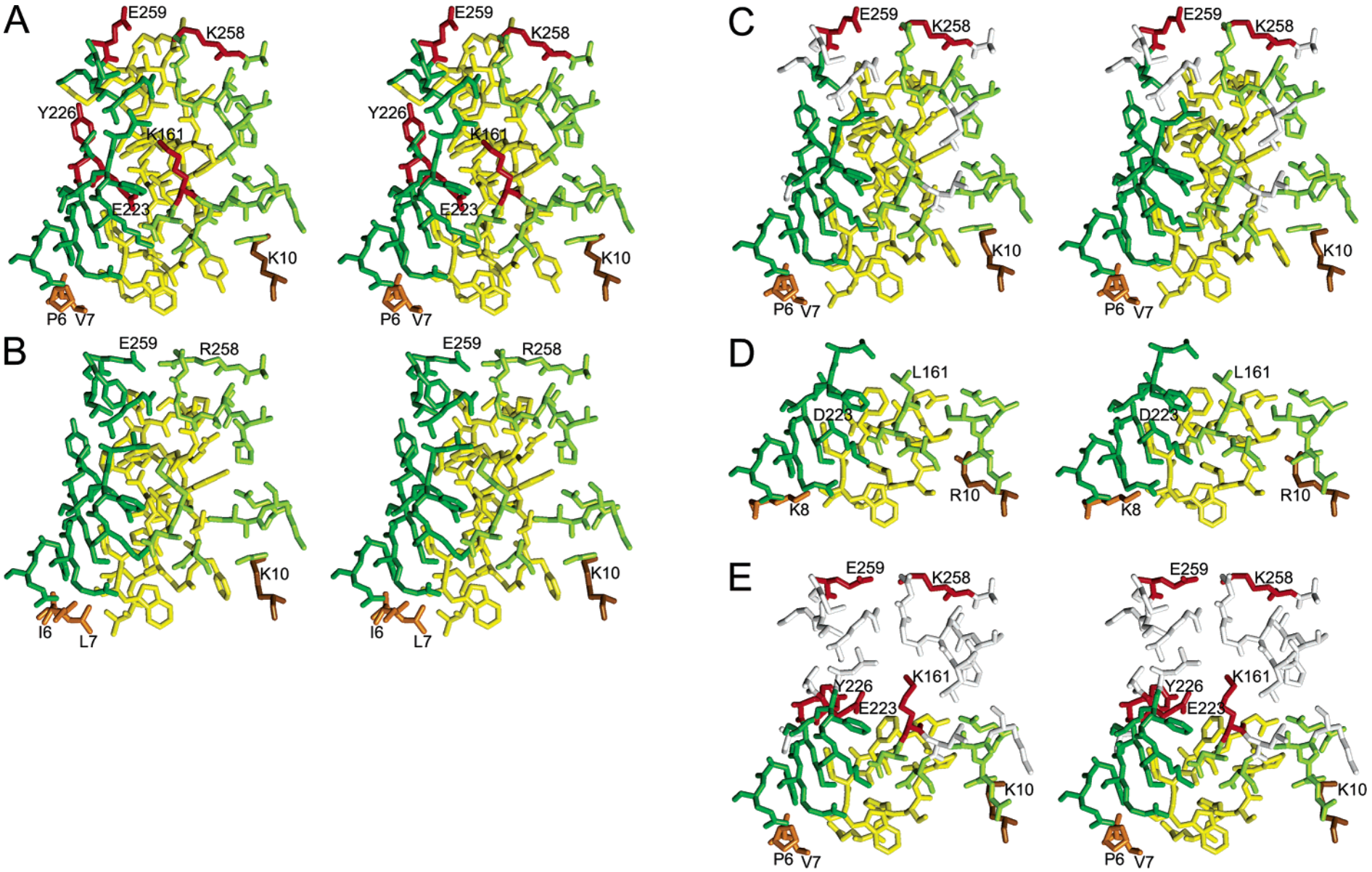

FIGURE 5: Stereoimages of residues surrounding the small-subunit βA$-\beta$B loops (yellow) of Rubisco: (A) *Chlamydomonas* (1GK8) (*14*), (B) spinach (8RUC) (*15*), (C) chimeric mutant ABSO, (D) *Synechococcus* (1RBL) (*16*), and (E) chimeric mutant ABAN. The central solvent channel is behind the structures. Large-subunit residues within 4.5 Å of the small-subunit βA$-\beta$B loops are colored light and dark green from neighboring subunits. Large-subunit residues in *Chlamydomonas* Rubisco that are not within 4.5 Å of the βA$-\beta$B loop in ABSO or ABAN Rubisco are colored gray. Large-subunit residues that show the greatest deviation in side-chain conformation between *Chlamydomonas* and ABSO or ABAN are colored red. Selected amino-terminal residues from a neighboring small subunit are colored orange, and those in the same small subunit as the βA$-\beta$B loop are colored brown. Residues are numbered according to their actual positions in the primary structures of the individual proteins.

The position of these residues appears to be influenced by differences in the interactions with the amino-terminal residues of the neighboring small subunit. Whereas *Chlamydomonas* and ABSO have Pro6 and Val7 (Figure 5A,C), spinach contains Ile6 and Leu7 in the same relative positions (Figure 5B). Despite these alterations, no differences are observed in the side chains of nearby large-subunit residues relative to the wild-type *Chlamydomonas* enzyme structure (*14*) or in the side chains of other βA−βB-loop residues relative to the spinach enzyme structure (*15*). Calculation of subunit surface area occluded by the ABSO and spinach βA−βB loops yielded quite similar values of 436 and 449 Å^2, respectively. These values are less than that for the βA−βB loop of wild-type *Chlamydomonas* (713 Å^2), but much of this difference is accounted for by the smaller size and lack of loop-to-loop contacts of the spinach loop.

The Cα backbone conformation of the ABAN βA−βB loop is also very similar to that of the native *Synechococcus* loop (Figure 5D,E). However, the ABAN loop residues are displaced by an average of 1 Å with a maximum displacement of 1.4 Å at Glu52. This displacement results from differences in the packing of the loop to amino-terminal residues in the same and in an adjacent small subunit. These, in turn, may be influenced by the longer carboxyl terminus of the *Chlamydomonas* small subunit. Lys8 in *Synechococcus* forms an ionic bond with Glu46 (Figure 5D) in a neighboring small subunit, but Pro6 and Val7 in ABAN (and wild-type *Chlamydomonas*) cause the side chain of Glu46 to interact with solvent (Figure 5A,E). On the opposite side of the βA−βB loop, van der Waals contacts between loop residues (Ser48, Asn49, Pro50) and the Arg10 side chain (in the same small subunit) of *Synechococcus* are lost in ABAN (which contains Lys10) (Figure 5D,E). These alterations result in a 21% decrease in the surface area occluded by the βA−βB loop from a value of 220 Å^2 in *Synechococcus* Rubisco to 173 Å^2 in the ABAN enzyme. Altogether, these differences in the structure of the βA−βB loop likely contribute to the thermal instability of the ABAN enzyme (Figures 3 and 4).

Specific Alterations in the Large Subunits. Because the large subunit contains the active site, and the ABSO and ABAN chimeric enzymes have altered kinetic properties relative to wild-type *Chlamydomonas* Rubisco (Table 1), one would anticipate that the foreign βA−βB loops would cause alterations in the large subunits. However, no significant differences in large-subunit Cα backbone atoms are observed among the wild-type, ABAN, and ABSO structures. Although the large subunits of *Chlamydomonas*, *Synechococcus*, and spinach are ∼90% identical in sequence, there are some large-subunit residues in contact with the small-subunit βA−βB loop that differ among them. It is among these residues that the greatest differences are observed when the *Chlamydomonas* wild-type, ABSO, and ABAN Rubisco structures are compared.

In the wild-type *Chlamydomonas* enzyme (*14*), Lys258 interacts with the small-subunit βA−βB loop by forming a van der Waals contact with the side chain of Val63 and a hydrogen bond with the carbonyl oxygen of Ser62. Lys258 also forms an intrasubunit hydrogen bond with large-subunit Asn287 and a solvent-mediated intersubunit hydrogen bond with Glu259 in an adjacent large subunit. The effect of the shorter βA−βB loops in the ABSO and ABAN chimeric enzymes is to abolish the intersubunit interactions of Lys258 with Ser62 and Val63. Thus, in the ABSO and ABAN enzymes (Figure 5C,E), Lys258 and Glu259 have greater conformational freedom, and the distance between them can be shortened relative to that of wild-type *Chlamydomonas* Rubisco (Figure 5A). The interactions of Lys258 and Glu259 in the ABAN structure are identical to those of Lys258 and Glu259 in the *Synechococcus* enzyme (*16*). In Rubisco from spinach, Arg258 forms an ionic bond with Glu259 from an adjacent large subunit (Figure 5B) and lacks the hydrogen bond with Asn287. In a previous study (*53*), a K258R substitution, in combination with other substitutions (C256F and I265V) that introduce residues characteristic of land plants, caused a decrease in Ω of *Chlamydomonas* Rubisco. Thus, although small, the variation in the Lys258 and Glu259 side chains observed in the ABSO and ABAN structures may contribute to the altered catalytic properties of the chimeric enzymes (Table 1).

In the *Chlamydomonas* enzyme (Figure 6A), the carbonyl oxygen of large-subunit Lys161 forms a hydrogen bond with the guanidino group of small-subunit Arg71. The carboxyl group of Glu223 (in a second large subunit) hydrogen bonds with both the guanidino group and carbonyl oxygen of Arg71 (Figure 6A). Arg71, in turn, forms a hydrogen bond with the carbonyl oxygen of Leu66 (Gly60 in spinach) in the core of the small-subunit βA−βB loop. In the *Synechococcus* enzyme (Figure 6B), all of these interactions are absent because Arg71 is replaced by Phe53. Furthermore, whereas *Chlamydomonas* Rubisco has large-subunit Lys161, large-subunit Glu223, and small-subunit Leu66, *Synechococcus* has large-subunit Leu161 and Asp223 and is missing a residue homologous with small-subunit Leu66 due to the smaller size of the βA−βB loop. In the chimeric mutant ABAN enzyme (Figure 6C), a residue comparable to Leu66 is also missing, but because of the absence of many βA−βB-loop residues, the side chains of large-subunit Lys161 and Glu223 move into the central solvent channel (Figure 6A,C). This appears to cause a major reorientation of the Tyr226 side chain (His226 in *Synechococcus*, Figure 6B) that results in the loss of another set of hydrogen bonds. In wild-type *Chlamydomonas* Rubisco (*14*), Tyr226 hydrogen bonds with large-subunit Gly261 and Leu266, as well as with the guanidino group of the small-subunit βA−βB-loop residue Arg59, which is missing from the ABAN enzyme. Altogether, the disruption of a network of hydrogen bonds may contribute to the thermal instability of the ABAN chimeric mutant enzyme (Figure 4). In a previous study (*30*), an R71A substitution in the βA−βB loop of the *Chlamydomonas* enzyme also caused decreases in carboxylation catalytic efficiency, Ω, and holoenzyme thermal stability, similar to the properties of mutant ABAN Rubisco (Table 1).

Alterations in the Active Sites of the Chimeric Enzymes. When compared with wild-type *Chlamydomonas* Rubisco (*14*), a number of minor alterations are observed in the distances between large-subunit and CABP atoms in the active sites of the ABAN and ABSO chimeric mutant enzymes. Because these differences are quite small, it is difficult to conclude that they have any direct effect on catalysis. The largest differences are observed in the ABSO structure. For example, the side-chain oxygens of Thr173 and Ser379 are >0.2 Å farther away from CABP O2 and O4, respectively, and the Lys334 side-chain nitrogen is >0.2

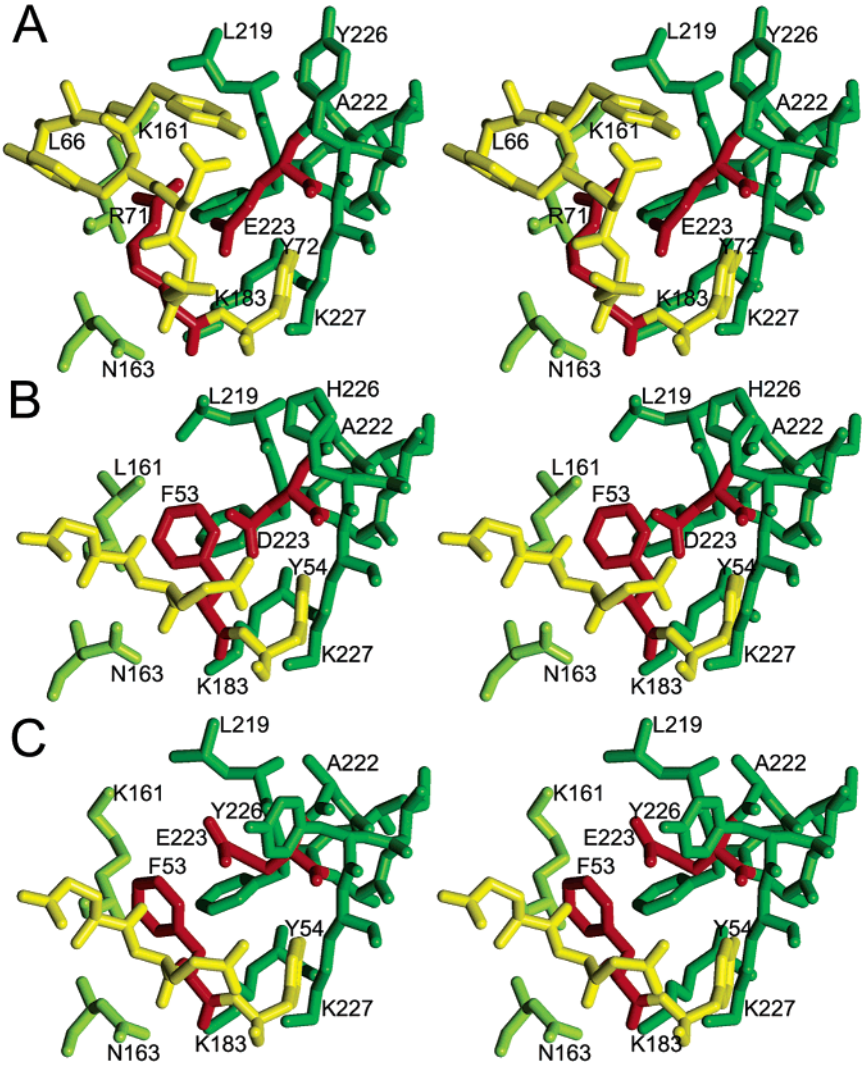

FIGURE 6: Stereoimages of selected residues in contact with the structurally homologous (in red) Rubisco small-subunit Arg71 and large-subunit Glu223 in *Chlamydomonas* (A), small-subunit Phe53 and large-subunit Asp223 in *Synechococcus* (B), and small-subunit Phe53 and large-subunit Glu223 in ABAN (C). These structures, with the central solvent channel in front, are rotated 180° around the *Y* axis relative to the images in Figure 5. Other small-subunit residues are colored yellow, and residues from neighboring large-subunits are colored light and dark green.

Å closer to CABP O3P. However, regardless of the significance of these small differences, no significant structural alterations are observed in the core of the ABAN and ABSO holoenzymes that may link active site alterations to changes observed in the regions surrounding the βA−βB loops.

DISCUSSION

By replacing the *Chlamydomonas* βA−βB loop with the shorter loops of *Synechococcus* (mutant ABAN) and spinach (mutant ABSO), it is readily apparent that the differences in size and residue identities are not essential for Rubisco holoenzyme assembly. Both chimeric enzymes assemble in vivo (Figure 3) and support the photosynthetic growth of *Chlamydomonas*, and both have βA−βB-loop structures nearly identical to those of the native *Synechococcus* and spinach Rubisco enzymes (Figure 5). Despite these observations, previous studies had indicated that the longer small-subunit loop of land plants was an essential holoenzyme "assembly domain" (*20*). It is likely that the lack of assembly of native *Synechococcus* small subunits with land plant large subunits may be due to an exaggeration of an inherent difficulty of holoenzyme assembly when small subunits are experimentally targeted to isolated chloroplasts (*20*−*22*).

In the present study, replacing the *Chlamydomonas* βA−βB loop with that of *Synechococcus* causes a decrease in holoenzyme thermal stability in vivo and in vitro (Figures 3 and 4), and the ABAN mutant strain has a temperature-conditional, acetate-requiring growth phenotype. The decrease in thermal stability may arise from a number of structural alterations observed in the crystal structure of ABAN Rubisco, including altered interactions between small-subunit amino-terminal residues and the βA−βB loop (Figure 5), as well as the loss of a network of hydrogen bonds resulting from a decrease in the size of the loop and the replacement of Arg71 by Phe (Figure 6). These alterations contribute to a 76% decrease in occluded surface area relative to the *Chlamydomonas* βA−βB loop and a 21% decrease relative to the native *Synechococcus* loop. Because surface areas occluded in the formation of protein complexes correlate highly with the free energies of protein−protein interactions (*54*), the decrease in occluded surface area can be viewed as an estimate of the relative thermodynamic

destabilization of the hexadecamer due to the introduction of the *Synechococcus* βA−βB loop.

Although no mutant substitution in the *Chlamydomonas* βA−βB loop has yet been found to eliminate Rubisco assembly or function, numerous studies have indicated that the nature of residues at the interface between large subunits and the small-subunit loops can influence holoenzyme thermal stability (*27*, *28*, *30*, *40*, *55*, *56*). Recently, X-ray crystal structures of large-subunit L290F mutant and L290F/A222T revertant enzymes have shown that substantial alterations in temperature factors occur for both large- and small-subunit residues in the βA−βB-loop region (*57*), thereby providing a physical basis for the effects of both large- and small-subunit substitutions that can either decrease or increase holoenzyme thermal stability (*28*, *30*, *56*). Thus, size of the loop is not entirely responsible for thermal stability. This is also apparent from the observation that the chimeric ABSO enzyme has a 39% decrease in occluded surface area relative to the βA−βB loop of *Chlamydomonas*, but the purified enzyme has a small increase in thermal stability in vitro (Figure 4).

Significant alterations in the catalytic properties of *Chlamydomonas* Rubisco were also observed for the ABSO and ABAN chimeric mutant enzymes (Table 1). In a previous study of *Chlamydomonas* Rubisco (*30*), changes in catalytic efficiency and specificity were observed when residues conserved in the green algal and land plant βA−βB loops were substituted with Ala. However, in the present study, the ABSO chimeric mutant enzyme was found to have decreases in V_c, K_c, and K_o despite the fact that the conserved residues are not altered. There must be some structural difference brought about by the introduction of the spinach loop, and this difference may account for the differences in catalytic properties between the native *Chlamydomonas* and spinach enzymes (*7*). In the ABSO crystal structure, only a minor change in the water-mediated hydrogen bonding of large-subunit residues Lys258 and Glu259 is observed at the apex of the small-subunit βA−βB loop (Figure 5). Nonetheless, when three substitutions were previously created in this large-subunit region (C256F, K258R, and I265V), which would introduce residues characteristic of land plant Rubisco, substantial decreases in carboxylation catalytic efficiency and Ω were observed (*53*). Perhaps a reduction in the size of the small-subunit βA−βB loop, like that of the ABSO chimeric mutant enzyme, would complement the detrimental catalytic effects of the large-subunit C256F/K258R/I265V triple-mutant enzyme.

The ABAN chimeric mutant enzyme has decreases in V_c and K_o that cause an 11% decrease in Ω (Table 1). In the ABAN crystal structure, as in the ABSO structure, the distance between Lys258 and Glu259 is decreased due to the shorter βA−βB loop. However, there are additional alterations in the side chains of large-subunit residues Lys161, Glu223, and Tyr226 that arise from the loss of their hydrogen-bonding partners Arg59 and Arg71 (Figure 6). Arg59 resides in a region of the *Chlamydomonas* βA−βB loop that is missing from the shorter *Synechococcus* loop, and Arg71 is replaced by Phe53. In a previous study (*30*), an R59A substitution in the *Chlamydomonas* βA−βB loop had little or no effect on the catalytic properties of Rubisco, but an R71A substitution caused increases in K_o and K_c and decreases in V_c and Ω. Furthermore, both substitutions caused a decrease in Rubisco thermal stability in vitro, but only the R71A mutant strain lacked holoenzyme and failed to grow photoautotrophically at the restrictive temperature of 35 °C. Thus, the altered catalytic properties and decreased thermal stability of ABAN Rubisco likely arise primarily from the substitution of Arg71 by Phe53 (Figure 6).

The small-subunit βA−βB loops are located in the central solvent channel of the holoenzyme where they interact with large subunits at the opposite ends of the α/β barrels that form the active sites (Figure 1). Despite this distant location, the introduction of the spinach and *Synechococcus* βA−βB loops into the *Chlamydomonas* small subunit causes significant changes in the catalytic properties of Rubisco. In the crystal structures of the ABSO and ABAN chimeric mutant enzymes, only small perturbations of questionable significance are observed in the active sites, and only a small number of the large-subunit side chains that are normally in contact with the *Chlamydomonas* βA−βB loop are altered by the foreign loops. Thus, one must consider that the introduction of the spinach and *Synechococcus* βA−βB loops affects the dynamic nature of the holoenzymes, and structural data alone may not be sufficient for elucidating the mechanisms that bring about the observed changes in catalysis. Nonetheless, it is clear that the small-subunit βA−βB loops can contribute to the differences in the catalytic properties of divergent Rubisco enzymes and may be worthy targets for further study aimed at engineering a superior Rubisco.

ACKNOWLEDGMENT

We thank Dr. Arminio Boschetti (University of Bern, Bern, Switzerland) for providing *Chlamydomonas* Rubisco antiserum.

REFERENCES

1. Spreitzer, R. J., and Salvucci, M. E. (2002) Rubisco: Structure, regulatory interactions, and possibilities for a better enzyme, *Annu. Rev. Plant Biol. 53*, 449−475.
2. Andersson, I., and Taylor, T. C. (2003) Structural framework for catalysis and regulation in ribulose-1,5-bisphosphate carboxylase/oxygenase, *Arch. Biochem. Biophys. 414*, 130−140.
3. Andrews, T. J., and Whitney, S. M. (2003) Manipulating ribulose bisphosphate carboxylase/oxygenase in the chloroplasts of higher plants, *Arch. Biochem. Biophys. 414*, 159−169.
4. Parry, M. A. J., Andralojc, R. A. C., Mitchell, P. J., Madgwick, P. J., and Keys, A. J. (2003) Manipulation of Rubisco: the amount, activity, function and regulation, *J. Exp. Bot. 54*, 1321−1333.
5. Spreitzer, R. J. (2003) Role of the Rubisco small subunit, *Arch. Biochem. Biophys*. *414*, 141−149.
6. Laing, W. A., Ogren, W. L., and Hageman, R. H. (1974) Regulation of soybean net photosynthetic CO_2 fixation by the interaction of CO_2, O_2 and ribulose 1,5-diphosphate carboxylase, *Plant Physiol. 54*, 678−685.
7. Jordan, D. B., and Ogren, W. L. (1981) Species variation in the specificity of ribulosebisphosphate carboxylase/oxygenase, *Nature 291*, 513−515.
8. Read, B. A., and Tabita, F. R. (1992) A hybrid ribulosebisphosphate carboxylase/oxygenase enzyme exhibiting a substantial increase in substrate specificity factor, *Biochemistry 31*, 5553−5559.
9. Read, B. A., and Tabita, F. R. (1994) High substrate specificity factor ribulose bisphosphate carboxylase/oxygenase from eukaryotic marine algae and properties of recombinant cyanobacterial Rubisco containing "algal" residue modifications, *Arch. Biochem. Biophys. 312*, 210−218.
10. Uemura, K., Anwaruzzaman, Miyachi, S., and Yokota, A. (1997) Ribulose-1,5-bisphosphate carboxylase/oxygenase from thermophilic red algae with a strong specificity for CO_2 fixation, *Biochem. Biophys. Res. Commun. 233*, 568−571.

11. Spreitzer, R. J. (1993) Genetic dissection of Rubisco structure and function, *Annu. Rev. Plant Physiol. Plant Mol. Biol. 43*, 411−434.
12. Kaplan, A., and Reinhold, L. (1999) CO_2 concentrating mechanisms in photosynthetic microorganisms, *Annu. Rev. Plant Physiol. Plant Mol. Biol. 50*, 539−570.
13. Edwards, G. E., Franceschi, V. R., and Voznesenskaya, E. V. (2004) Single-cell C4 photosynthesis versus the dual-cell (Kranz) paradigm, *Annu. Rev. Plant Biol. 55*, 173−196.
14. Taylor, T. C., Backlund, A., Bjorhall, K., Spreitzer, R. J., and Anderson, I. (2001) First crystal structure of Rubisco from a green alga, *Chlamydomonas reinhardtii*, *J. Biol. Chem. 276*, 48159−48164.
15. Andersson, I. (1996) Large structures at high resolution: The 1.6 Å crystal structure of spinach ribulose-1,5-bisphosphate carboxylase/oxygenase complexed with 2-carboxyarabinitol bisphosphate, *J. Mol. Biol. 259*, 160−174.
16. Newman, J., and Gutteridge, S. (1993) The X-ray structure of *Synechococcus* ribulose-bisphosphate carboxylase/oxygenase-activated quaternary complex at 2.2-Å resolution, *J. Biol. Chem. 268*, 25876−25886.
17. Schreuder, H. A., Knight, S., Curmi, P. M. G., Andersson, I., Cascio, D., Sweet, R. M., Branden, C. I., and Eisenberg, D. (1993) Crystal structure of activated tobacco rubisco complexed with the reaction-intermediate analogue 2-carboxyarabinitol 1,5-bisphosphate, *Protein Sci. 2*, 1136−1146.
18. Hansen, S., Vollan, V. B., Hough, E., and Andersen, K. (1999) The crystal structure of Rubisco from *Alcaligenes eutrophus* reveals a novel central eight-stranded β-barrel formed by β-strands from four subunits, *J. Mol. Biol. 288*, 609−621.
19. Sugawara, H., Yamamoto, H., Shibata, N., Inoue, T., Okada, S., Miyake, C., Yokota, A., and Kai, Y. (1999) Crystal structure of carboxylase reaction-oriented ribulose-1,5-bisphosphate carboxylase/oxygenase from a thermophilic red alga, *Galdieria partita*, *J. Biol. Chem. 274*, 15655−15661.
20. Wasmann, C. C., Ramage, R. T., Bohnert, H. J., and Ostrem, J. A. (1989) Identification of an assembly domain in the small subunit of ribulose-1,5-bisphosphate carboxylase, *Proc. Natl. Acad. Sci. U.S.A. 86*, 1198−1202.
21. Flachmann, R., and Bohnert, H. J. (1992) Replacement of a conserved arginine in the assembly domain of ribulose-1,5-bisphosphate carboxylase/oxygenase small subunit interferes with holoenzyme formation, *J. Biol. Chem. 267*, 10576−10582.
22. Adam, Z. (1995) A mutation in the small subunit of ribulose-1,5-bisphosphate carboxylase/oxygenase that reduces the rate of its incorporation into holoenzyme, *Photosynth. Res. 43*, 143−147.
23. Cloney, L. P., Bekkaoui, D. R., and Hemmingsen, S. M. (1993) Co-expression of plastid chaperonin genes and a synthetic plant Rubisco operon in *Escherichia coli*, *Plant Mol. Biol. 23*, 1285−1290.
24. Getzoff, T. P., Zhu, G., Bohnert, H. J., and Jensen, R. G. (1998) Chimeric *Arabidopsis thaliana* ribulose-1,5-bisphosphate carboxylase/oxygenase containing a pea small subunit protein is compromised in carbamylation, *Plant Physiol. 116*, 695−702.
25. Whitney, S., and Andrews, T. (2001) The gene for the ribulose-1,5-bisphosphate carboxylase/oxygenase (Rubisco) small subunit relocated to the plastid genome of tobacco directs the synthesis of small subunits that assemble into Rubisco, *Plant Cell 13*, 193−205.
26. Zhang, X. H., Ewy, R. G., Widholm, J. M., and Portis, A. R. (2002) Complementation of the nuclear antisense *rbcS*-induced photosynthesis deficiency by introducing an *rbcS* gene into the tobacco plastid genome, *Plant Cell Physiol. 43*, 1302−1313.
27. Chen, Z., Chastain, C. J., Al-Abed, S. R., Chollet, R., and Spreitzer, R. J. (1988) Reduced CO_2/O_2 specificity of ribulose-1,5-bisphosphate carboxylase/oxygenase in a temperature-sensitive chloroplast mutant of *Chlamydomonas reinhardtii*, *Proc. Natl. Acad. Sci. U.S.A. 85*, 4696−4699.
28. Du, Y. C., Hong, S., and Spreitzer, R. J. (2000) *RbcS* suppressors enhance the CO_2/O_2 specificity and thermal stability of *rbcL*-mutant ribulose-1,5-bisphosphate carboxylase/oxygenase, *Proc. Natl. Acad. Sci. U.S.A. 97*, 14206−14211.
29. Khrebtukova, I., and Spreitzer, R. J. (1996) Elimination of the *Chlamydomonas* gene family that encodes the small subunit of ribulose-1,5-bisphosphate carboxylase/oxygenase, *Proc. Natl. Acad. Sci. U.S.A. 93*, 13689−13693.
30. Spreitzer, R. J., Esquivel, M. G., Du, Y. C., and McLaughlin, P. D. (2001) Alanine-scanning mutagenesis of the small-subunit βA-βB loop of chloroplast ribulose-1,5-bisphosphate carboxylase/oxygenase: Substitution at Arg-71 affects thermal stability and CO_2/O_2 specificity, *Biochemistry 40*, 5615−5621.
31. Spreitzer, R. J., and Mets, L. (1981) Photosynthesis-deficient mutants of *Chlamydomonas reinhardtii* with associated light-sensitive phenotypes, *Plant Physiol. 67*, 565−569.
32. Yanisch-Perron, C., Vieira, J., and Messing, J. (1985) Improved M13 phage cloning and host strains: Nucleotide sequence of the M13 mp19 and pUC19 vectors, *Gene 33*, 103−119.
33. Shimogawara, K., Fujiwara, S., Grossman, A., and Usuda, H. (1998) High-efficiency transformation of *Chlamydomonas reinhardtii* by electroporation, *Genetics 148*, 1821−1828.
34. Newman, S. M., Boynton, J. E., Gillham, N. W., Randolph-Anderson, B. L., Johnson, A. M., and Harris, E. H. (1990) Transformation of chloroplast ribosomal RNA genes in *Chlamydomonas*: Molecular and genetic characterization of integration events, *Genetics 126*, 875−888.
35. Bradford, M. M. (1976) A rapid and sensitive method for the quantitation of microgram quantities of protein utilizing the principle of protein-dye binding, *Anal. Biochem. 72*, 248−254.
36. Spreitzer, R. J., and Chastain, C. J. (1987) Heteroplasmic suppression of an amber mutation in the *Chlamydomonas* chloroplast gene that encodes the large subunit of ribulosebisphosphate carboxylase/oxygenase, *Curr. Genet. 11*, 611−616.
37. Chua, N. H. (1980) Electrophoretic analysis of chloroplast proteins, *Methods Enzymol. 69*, 434−446.
38. Gotor, C., Hong, S., and Spreitzer, R. J. (1994) Temperature-conditional nuclear mutation of *Chlamydomonas reinhardtii* decreases the CO_2/O_2 specificity of chloroplast ribulosebisphosphate carboxylase/oxygenase, *Planta 193*, 313−319.
39. Werneke, J. M., Zielinski, R. E., and Ogren, W. L. (1988) Structure and expression of spinach leaf cDNA encoding ribulosebisphosphate carboxylase/oxygenase activase, *Proc. Natl. Acad. Sci. U.S.A. 85*, 787−791.
40. Chen, Z., Hong, S., and Spreitzer, R. J. (1993) Thermal instability of ribulose-1,5-bisphosphate carboxylase/oxygenase from a temperature-conditional chloroplast mutant of *Chlamydomonas reinhardtii*, *Plant Physiol. 101*, 1189−1194.
41. Jordan, D. B., and Ogren, W. L. (1981) A sensitive assay procedure for simultaneous determination of ribulose-1,5-bisphosphate carboxylase and oxygenase activity, *Plant Physiol. 67*, 237−245.
42. Spreitzer, R. J., Jordan, D. B., and Ogren, W. L. (1982) Biochemical and genetic analysis of an RuBP carboxylase/oxygenase-deficient mutant and revertants of *Chlamydomonas reinhardtii*, *FEBS Lett. 148*, 117−121.
43. Kuehn, G. D., and Hsu, T. C. (1978) Preparative-scale enzymic synthesis of D-[^{14}C]ribulose 1,5-bisphosphate, *Biochem. J. 175*, 909−912.
44. Otwinowski, Z., and Minor, W. (1997) Processing of X-ray diffraction data collected in oscillation mode, *Methods Enzymol. 276*, 307−326.
45. Navaza, J., and Saludjian, P. (1997) AMoRe: An automated molecular replacement program package, *Methods Enzymol. 276*, 581−594.
46. Collaborative Computational Project, Number 4 (1994) The CCP4 suite−programs for protein crystallography, *Acta Crystallogr. D50*, 760−763.
47. Murshudov, G. N., Vagin, A. A., and Dodson, E. J. (1997) Refinement of macromolecular structures by the maximum-likelihood method, *Acta Crystallogr. D53*, 240−255.
48. Perrakis, A., Sixma, T. K., Wilson, K. S., and Lamzin, V. S. (1997) wARP: Improvement and extension of crystallographic phases by weighted averaging of multiple-refined dummy atomic models, *Acta Crystallogr. D53*, 448−455.
49. Pannu, N. S., and Read, R. J. (1996) Improved structure refinement through maximum likelihood, *Acta Crystallogr. A52*, 659−668.
50. Jones, T. A., Zou, J.-Y., Cowan, S. W., and Kjeldgaard, M. (1991) Improved methods for building protein models in electron-density maps and the location of errors in these models, *Acta Crystallogr. A47*, 110−119.
51. Pattabiraman, N., Ward, K. B., and Fleming, P. J. (1995) Occluded molecular surface: Analysis of protein packing, *J. Mol. Recognit. 8*, 334−344.
52. Spreitzer, R. J., Goldschmidt-Clermont, M., Rahire, M., and Rochaix, J. D. (1985) Nonsense mutations in the *Chlamydomonas* chloroplast gene that codes for the large subunit of ribulosebisphosphate carboxylase/oxygenase, *Proc. Natl. Acad. Sci. U.S.A. 82*, 5460−5464.

53. Du, Y. C., Peddi, S. R., and Spreitzer, R. J. (2003) Assessment of structural and functional divergence far from the large-subunit active site of ribulose-1,5-bisphosphate carboxylase/oxygenase, *J. Biol. Chem. 278*, 49401−49405.
54. Fleming, K. G., Ackerman, A. L., and Engelman, D. M. (1997) The effect of point mutations on the free energy of transmembrane alpha-helix dimerization, *J. Mol. Biol. 272*, 266−275.
55. Hong, S., and Spreitzer, R. J. (1997) Complementing substitutions at the bottom of the barrel influence catalysis and stability of ribulose-bisphosphate carboxylase/oxygenase, *J. Biol. Chem. 272*, 11114−11117.
56. Du, Y. C., and Spreitzer, R. J. (2000) Suppressor mutations in the chloroplast-encoded large subunit improve the thermal stability of wild-type ribulose-1,5-bisphosphate carboxylase/oxygenase, *J. Biol. Chem. 275*, 19844−19847.
57. Karkehabadi, S., Taylor, T. C., Spreitzer, R. J., and Andersson, I. (2005) Altered intersubunit interactions in crystal structures of catalytically compromised ribulose-1,5-bisphosphate carboxylase/oxygenase, *Biochemistry 44*, 113−120.

BI050537V